PCCP

Accepted Manuscript

ROYAL SOCIETY OF CHEMISTRY

www.rsc.org/pccp

Adiabatic ionization energies of the overlapped A^2A_1 and B^2E electronic states in CH_3Cl^+/CH_3F^+ measured with double imaging electron/ion coincidence

Xiaofeng Tang*, Gustavo A. Garcia, and Laurent Nahon

Synchrotron SOLEIL, L'Orme des Merisiers, St. Aubin BP 48, 91192 Gif sur Yvette, France

Abstract

Utilizing vacuum ultraviolet (VUV) synchrotron radiation and double imaging photoelectron photoion coincidence (i^2PEPICO) technique, we have measured the adiabatic ionization energies (AIEs) of the overlapped A^2A_1 and B^2E electronic states of CH_3Cl^+ and CH_3F^+ ions. We show that the two overlapped electronic states can be separated in the electron and ion kinetic energy correlation diagrams based on their state-specific dissociation dynamics, leading to different kinetic energies released in dissociation, along the CH_3^+ fragmentation channel. Thus the correlation diagrams yield values of 13.67 $\pm$ 0.03 and 14.77 $\pm$ 0.03 eV for the AIEs of the A^2A_1 and B^2E states of CH_3Cl^+, and 16.08 $\pm$ 0.03 and 17.00 $\pm$ 0.05 eV for CH_3F^+, respectively. This method can be generalized to separate ionic states that are otherwise overlapped in normal photoelectron spectra (PES), especially by combining VUV sources and electron/ion coincidence techniques.

*Corresponding author. E-mail: xiaofeng.tang@synchrotron-soleil.fr

1. Introduction

Photoelectron spectroscopy (PES) is a commonly used and precious tool to unravel the molecular electronic structure.[1, 2] Besides, photoionization experiments provide valuable energetic information such as ionization energy and fragment appearance energy, which play an essential role in thermochemistry and have been used in a wide range of areas.[3-11] This long lasting experimental effort has also promoted the development of high level quantum chemical computation procedures.[12, 13]

The determination of accurate ionization energy and appearance energy has made considerable progresses with the popular methods of photoionization mass spectrometry (PIMS) and PES coupled to modern light sources like vacuum ultraviolet (VUV) laser and synchrotron radiation.[3, 4, 14] Especially the techniques of threshold photoelectron spectroscopy (TPES) and threshold photoelectron photoion coincidence (TPEPICO) have been frequently employed to measure the values of ionization energy and fragment appearance energy due to the high collection efficiency of threshold electrons associated to a high and constant electron energy resolution.[15-21]

Despite these experimental progresses, in some cases electron spectroscopy is unable to decipher electronic states. Indeed, in photoionization process the molecular ions may be prepared in different states depending on the photon energy and transition possibility. The electronic structures of excited ionic states are often more complicated than the ground state and may be involved in many phenomena such as dissociation, fluorescence and autoionization. Especially for the overlapped states commonly existing in the excited electronic states[1, 4], due to the small energy difference between them, it is still a challenge for both experimental and theoretical scientists to accurately measure or predict their ionization energies.

This is precisely the situation encountered for the two target molecules of this paper, methyl halides CH_3Cl and CH_3F, which are also important chemical reagents with a high-symmetry structure (C_{3V}) and have attracted a lot of attention in the past decades.[22-34] The valence shell molecular configurations of CH_3Cl and CH_3F in their X^1A_1 electronic ground state are known as $(1a_1)^2(2a_1)^2(1e)^4(3a_1)^2(2e)^4$, where their core shells have been neglected for simplicity.[26] The X^2E, A^2A_1 and B^2E ionic states, obtained by removing one electron from the 2e, $3a_1$ and 1e orbitals of the neutral X^1A_1 ground state, respectively, are considered to be the three low-lying electronic states of CH_3Cl^+ and CH_3F^+ ions. The X^2E ground states of both CH_3Cl^+ and CH_3F^+, have vibrational structures visible in their PES[33] and TPES[22, 23] and their adiabatic ionization energies (AIEs) locate at 11.289 ± 0.003 and 12.533 ± 0.006 eV[33], respectively. The A^2A_1 and B^2E electronic excited states exhibit a broad and structureless band in the PES[33] and TPES[22, 23]. The A^2A_1 and B^2E states of CH_3Cl^+ partially overlap and those of CH_3F^+ totally overlap, due to a small energy difference between them and the natural width of the dissociative states, so that they cannot be separated even with high resolution electron spectroscopy, a situation frequently encountered in other molecular systems[1]. The AIE and vertical ionization energy (VIE) of the A^2A_1 state of CH_3Cl^+ were measured at 13.8 and 14.4 eV, and the VIE of B^2E at 15.4 eV,[33] but to our knowledge the AIE of the B^2E states has never been measured. The AIE and VIE of the totally overlapped A^2A_1 and B^2E band of CH_3F^+ locate at 16.3 and 17.2 eV.[33] It is thus challenging to separate and accurately measure their individual ionization energies.

Both the A^2A_1 and B^2E electronic states are dissociative and CH_3^+ is the main fragment ion in the dissociation of CH_3Cl^+ and CH_3F^+ ions.[22, 23, 32] The appearance energies of CH_3^+ fragment ions in the dissociation of CH_3Cl^+ and CH_3F^+ are at 13.38 and 14.54 eV, respectively, lying in the Franck-Condon gap. In addition, previous studies have shown that the dissociation of CH_3Cl^+ and CH_3F^+ ions in the different electronic states along the CH_3^+

formation channel is state-specific, even outside of the Franck-Condon region.[22, 23, 32] So it is possible to separate the overlapped A^2A_1 and B^2E states based on their different dissociation dynamics.

Using VUV synchrotron radiation and a double imaging photoelectron photoion coincidence (i^2PEPICO) spectrometer[18], we have measured the ionization energies of the overlapped A^2A_1 and B^2E states of CH_3Cl^+ and CH_3F^+ ions based on their different dissociation dynamics which can be clearly observed from the electron and ion kinetic energy correlation diagrams[29, 35, 36].

2. Experimental

The experiments were performed with an i^2PEPICO spectrometer, DELICIOUS III[18], on the VUV beamline DESIRS[37] at Synchrotron SOLEIL, France. The detailed configurations of DELICIOUS III and synchrotron beamline have already been introduced before, and so only a brief description is provided here. Synchrotron photons emitted from an undulator were dispersed by a 6.65 m normal incidence monochromator. A 200 l/mm grating was chosen and the monochromator slits were set to provide a photon energy resolution of ~3 meV. A gas filter filled with Ar for $h\nu < 15.5$ eV was used to suppress the high harmonics emitted from the undulator. The absolute synchrotron photon energy has been calibrated within an accuracy of ± 1 meV by using the absorption lines of Ar in the gas filter seen as dips in the ionization signal during the energy scans. Pure CH_3Cl (CH_3F, commercially obtained from Synquest Laboratories) seeded in Ne (He) carrier gas with a volume ratio of 1:49 was expanded through a 50 μm diameter nozzle and collimated by a skimmer (Beam Dynamics, 1.0 mm diameter) to form a continuous molecular beam. The molecular beam crossed the synchrotron light at a right angle in the center of DELICIOUS III, and the electrons and ions produced in photoionization were extracted and accelerated in opposite directions by an electric field. A velocity map imaging (VMI)[38] and a modified Wiley-McLaren time-of-flight

(TOF)[39] imaging spectrometers were employed to detect electrons and ions, respectively. PES and electron angular distributions were obtained from the electron VMI image via an Abel inversion algorithm[40], while the full ion 3D momentum distribution was extracted from the ion TOF and the 2D arrival position onto the corresponding position-sensitive detector (PSD). The coincidence scheme yielded electron images, and thus PES, correlated to a particular mass and ion momentum, which in turn produced the electron and ion kinetic energy correlation diagram[29, 35, 36]. A subtraction method[17, 41] was employed to get TPES and TPEPICO spectra. The photon flux was measured with a photodiode (AXUV100, IRD) and was used to normalize the photon energy scans.

3. Results and discussion

3.1 TPES and TPEPICO spectra

TPES of CH_3Cl in the 11.0-17.1 eV and CH_3F in the 12.2-19.8 eV energy ranges were measured with a 10 meV step size and are presented as black solid lines in Figure 1(a) and (b). The X^2E, A^2A_1 and B^2E three low-lying electronic states of CH_3Cl^+ and CH_3F^+ ions can be prepared and have been assigned in the TPES.[22, 23] For both CH_3Cl^+ and CH_3F^+, their X^2E electronic ground states exhibit vibrational structures and their AIEs have been determined at 11.30 ± 0.01 and 12.56 ± 0.01 eV, which are in agreement with previous results.[22, 23, 33] However, unlike the PES recorded at fixed photon energy[33], the TPES in the Franck-Condon gap are not vanishing leading to a non-negligible ion production. This can be explained by the well-known fact that, besides direct photoionization, TPES may also have contributions from indirect processes such as autoionization. Therefore the high vibrational levels of the X^2E ground state in the Franck-Condon gap are populated via the autoionization of neutral Rydberg states.[22]

The A^2A_1 and B^2E electronic excited states exhibit a broad and structureless band in the TPES. For CH_3Cl^+ ions, due to the effect of autoionization, the small valley between the

A^2A_1 and B^2E states observed in previous He(I) PES[33] is not as obvious in the TPES. The A^2A_1 and B^2E states partially overlap in the TPES and their VIEs are measured at 14.6 and 15.3 eV. The A^2A_1 and B^2E states of CH_3F^+ totally overlap and the peak of the overlapped band locates at 17.2 eV. These data agree well with previous results.[22, 23, 33] Due to the small energy gap and natural peak widths, the overlapped A^2A_1 and B^2E states cannot be separated in the TPES even with a higher energy resolution.

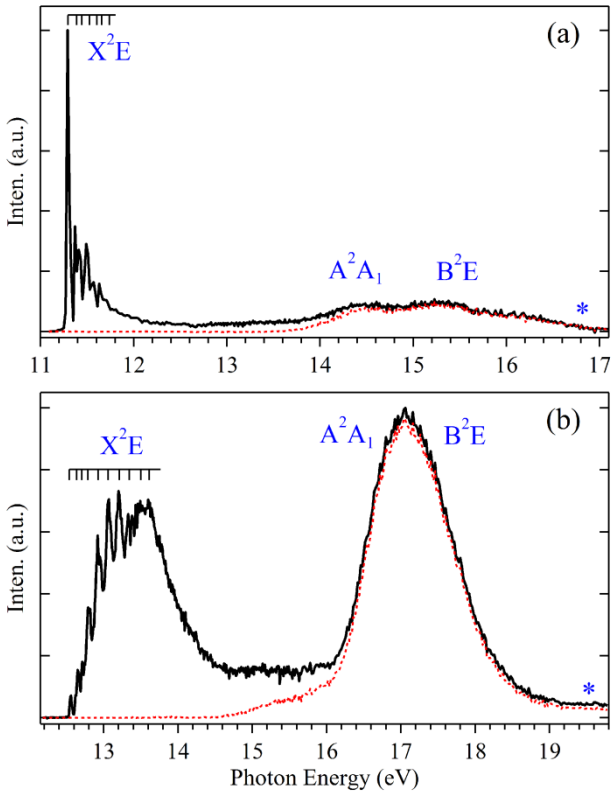

FIG. 1. TPES (black solid lines) of (a) CH_3Cl and (b) CH_3F and mass-selected TPEPICO spectra (red dotted lines) of CH_3^+ fragment ions. Two photon energies at hν = 16.80 and 19.50 eV at which fixed coincidence experiments were performed are marked with stars.

Previous results have shown that the A^2A_1 and B^2E states of CH_3Cl^+ and CH_3F^+ ions are dissociative and CH_3^+ is the predominant fragment ion in their dissociation.[22, 23, 32] The mass-selected TPEPICO spectra of the CH_3^+ fragment ion were also measured and are shown as red dotted lines in Figure 1. From the first point above the noise, the appearance energy of the CH_3^+ fragment ion dissociated from CH_3Cl^+ (CH_3F^+) has been measured and locates at 13.43 ±0.01 eV (14.58 ±0.01 eV), lying in the Franck-Condon gap. The curves in Figure 1 indicate

that nearly all the CH_3Cl^+ (CH_3F^+) ions in the A^2A_1 and B^2E states dissociate to CH_3^+ and Cl (F) fragments. In the TPEPICO spectra the A^2A_1 and B^2E states still overlap and cannot be separated.

3.2 CH_3^+ formation in dissociation of CH_3Cl^+ at hv = 16.80 eV

The dissociation mechanism of energy-selected CH_3Cl^+ ions has already been studied in detail by the method of TPEPICO imaging,[20, 23] where it was shown that the dissociation of the CH_3Cl^+ ions in different electronic states is state-specific. The A^2A_1 first excited state is a repulsive state along the CH_3^+ fragmentation channel and the dissociation is direct and fast. Unlike the A^2A_1 state, the kinetic energy of the CH_3^+ fragment ion dissociated from the B^2E state is small and can be fitted with a Boltzmann function, which indicates that the dissociation of the B^2E state is statistical and proceeds via internal conversion to the high vibrational levels of the X^2E ground state.[23] It is then possible to separate the overlapped A^2A_1 and B^2E states based on their different dissociation mechanisms, leading to different kinetic energies released (KERs) in the dissociation, along the CH_3^+ fragmentation channel.

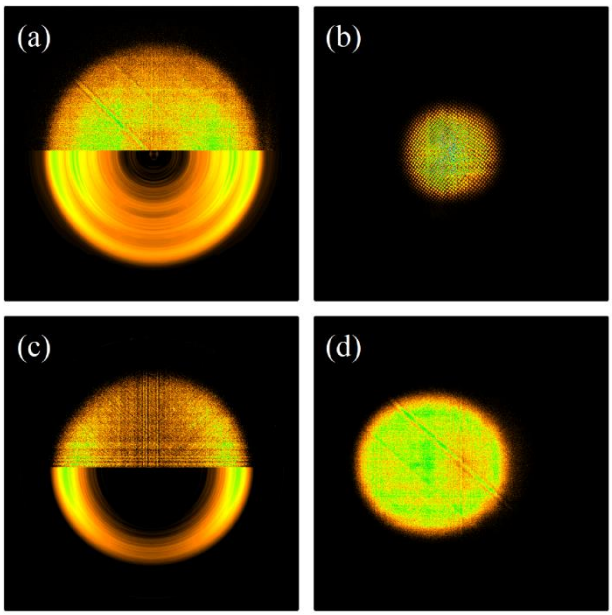

FIG. 2. Mass-selected (a) electron and (b) ion images corresponding to the CH_3^+ fragment ions in dissociative photoionization of CH_3Cl at hν = 16.80 eV; The same (c) electron and (d) ion images in dissociative photoionization of CH_3F at hν = 19.50 eV. The lower half part of the electron images corresponds to the result from the image inversion pBasex algorithm.

The mass-selected electron and ion images corresponding to the CH_3^+ fragment ion dissociated from CH_3Cl^+ ion were recorded at the fixed photon energy hν = 16.80 eV and are displayed in Figure 2(a) and (b). The upper half part of the electron image represents the raw data and the lower corresponds to the results from the pBasex inversion algorithm[40]. Two rings corresponding to the A^2A_1 and B^2E states can be discerned with an obvious anisotropic distribution and partially overlap in the electron image. The CH_3^+ ion image exhibit a large diameter circular pattern indicating that a large kinetic energy has been released in the dissociation.

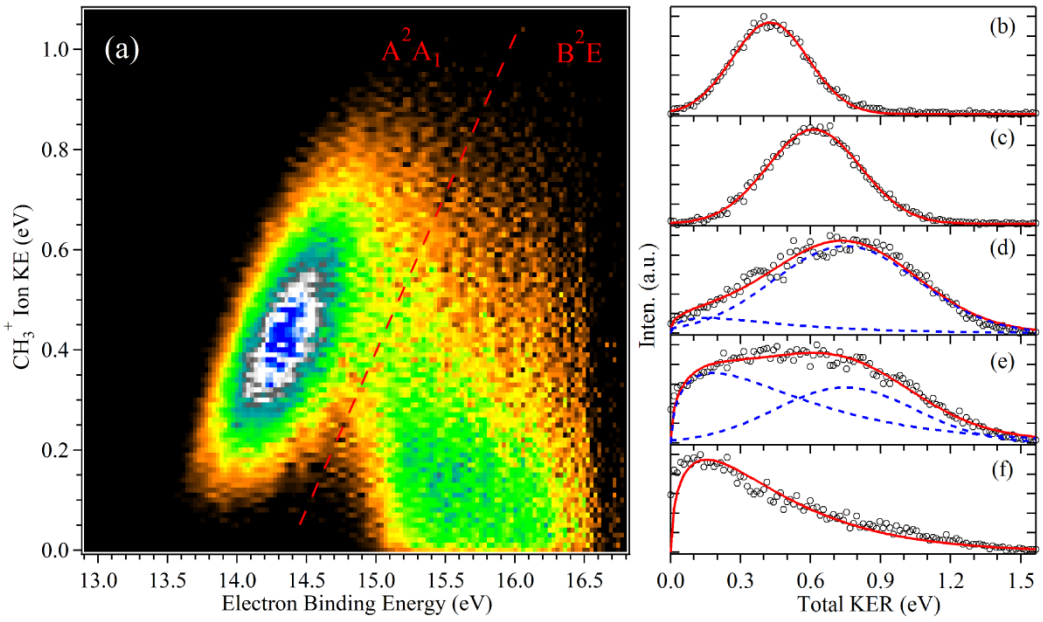

FIG. 3. (a) Electron and ion kinetic energy correlation diagram in the dissociation of CH_3Cl^+ along the CH_3^+ fragmentation channel recorded at hν = 16.80 eV; (b)-(f) Total center of mass KER of the CH_3^+ and Cl fragments in the dissociation of CH_3Cl^+ at selected electron binding energies of 14.00, 14.40, 14.90, 15.10 and 15.90 eV, the black dots represent the raw data, and the red solid lines correspond to the fitted results with Boltzmann and/or Gaussian functions (blue dotted lines).

By combining the electron and ion images in coincidence, the electron and ion kinetic energy correlation diagram is obtained and displayed in Figure 3(a). It is shown that the CH_3Cl^+ ions can be prepared in the 13.5-16.8 eV electron binding energy range with the hν = 16.80 eV photons, including the A^2A_1 and B^2E states, which then dissociate to the CH_3^+ fragment ions. The contour of the correlation diagram can be divided into two parts, an

intense part with electron binding energies of 13.5 ~ 14.8 eV and a weak part with electron binding energies of 14.8 ~ 16.8 eV. For the intense part, the KER in the fragmentation presents a nearly linear increase with the binding energy, consistent with a dissociative potential energy surface, while for electron binding energies above 15 eV, the KER loses this dependency and dramatically peaks at low KER.

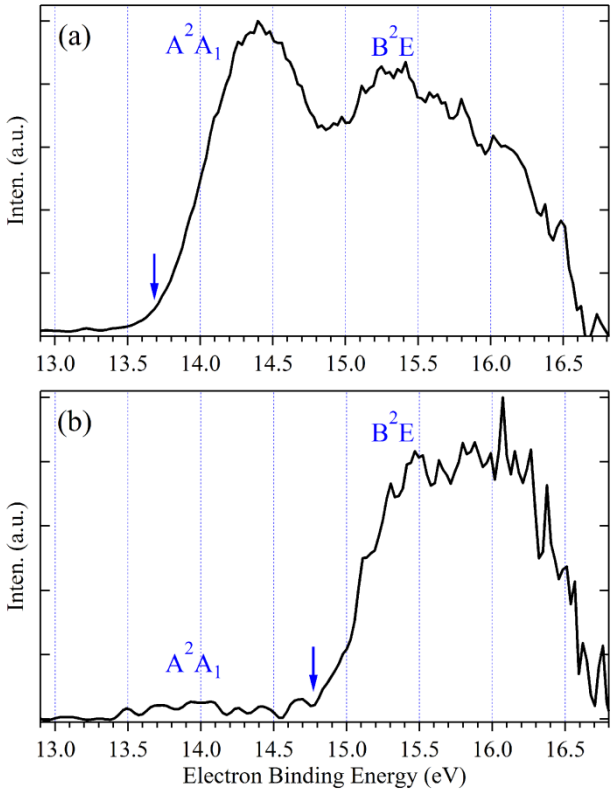

FIG. 4. (a) KER(CH_3^+) < 0.8 eV and (b) KER(CH_3^+) < 0.1 eV kinetic energy filtered PES of CH_3Cl recorded at hν = 16.80 eV. The AIEs of the A^2A_1 and B^2E states of CH_3Cl^+ are also marked with arrows in the figure.

The total center of mass KERs of the CH_3^+ and Cl fragments dissociated from energy-selected CH_3Cl^+ ions with electron binding energies of 14.00, 14.40, 14.90, 15.10 and 15.90 eV are presented in Figure 3(b~f). The shape of the total KER curves changes with electron binding energy. The KER curves at lower binding energies of Figures 3(b) and (c) suggest a large kinetic energy and are fitted well with a Gaussian function. They correspond to the intense part of the correlation diagram and are attributed to the fast direct dissociation of the A^2A_1 state.[23] At higher electron binding energy, in Figure 3(d) and (e), an additional

Boltzmann function is needed to the fit of the total KER curves, corresponding to the weak part of the correlation diagram and to the statistical dissociation of the B^2E state,[23] whose intensity increases with binding energy and dominates above 15.9 eV, as seen in Figure 3(f). The overlapped A^2A_1 and B^2E states of CH_3Cl^+ therefore have been separated successfully in the correlation diagram based on their different dissociation mechanisms along the CH_3^+ fragmentation channel.

The correlation diagram in Figure 3(a) can also be projected along the electron kinetic energy (electron binding energy) axis for a given ion KER to yield PES filtered in ion mass and kinetic energy. These projections can be used to maximize the separation of the A^2A_1 and B^2E states by their different KERs. For example, the iKE-filtered PES with KER(CH_3^+) < 0.8 eV was extracted from the correlation diagram and presented in Figure 4(a). Both the A^2A_1 and B^2E states of CH_3Cl^+ can be identified in the iKE-filtered PES. Although the overall shape is similar to the TPES of Figure 1(a), some differences can be identified in the PES, for example, a near zero intensity in the Franck-Condon gap between the X^2E and A^2A_1 states, a large intensity of the A^2A_1 state and the deeper valley between the A^2A_1 and B^2E states, which should be ascribed to the effect of autoionization in the TPES and the partial photoionization cross section dependence on photon energy. The AIE of the A^2A_1 state is measured at 13.67 $\pm$ 0.03 eV by linear extrapolation and indicated with an arrow in the iKE-filtered PES. Furthermore, by selecting the KER(CH_3^+) with a maximum value of 0.1 eV, the iKE-filtered PES was extracted again and is shown in Figure 4(b). Now only one band corresponding to the B^2E state appears in the PES, with a negligible intensity for the A^2A_1 state. From the iKE-filtered PES, the AIE of the B^2E state has been accurately measured for the first time at 14.77 $\pm$ 0.03 eV.

3.3 CH_3^+ formation in dissociation of CH_3F^+ at hv = 19.50 eV

Similar to the case of CH_3Cl^+, the dissociation of CH_3F^+ ions in the different electronic states is also state-specific[32], even outside the Franck-Condon region. The detailed dissociation mechanism of CH_3F^+ has also already been discussed in our recent publication by using the method of i^2PEPICO.[22] The A^2A_1 first excited state of CH_3F^+ is still a repulsive state along the CH_3^+ fragmentation channel and the dissociation of the B^2E state is also statistical. So the above method can be employed to separate and measure the ionization energies of the overlapped A^2A_1 and B^2E states of CH_3F^+ too.

The mass-selected electron and ion images corresponding to the CH_3^+ fragment ion dissociated from CH_3F^+ ion were recorded at the fixed photon energy hν = 19.50 eV and are displayed in Figure 2(c) and (d). Only one ring can be seen in the electron image, consistent with the fact that the A^2A_1 and B^2E states totally overlap. By combining together the electron and ion images, the electron and ion kinetic energy correlation diagram is obtained and shown in Figure 5(a). Similar to our previous results performed at hν = 18.50 eV[22], the present correlation diagram also consists of two parts, a weak part with KER(CH_3^+) < 0.4 eV and an intense part with KER(CH_3^+) = 0.4 ~ 1.7 eV. The total center of mass KERs of CH_3^+ and F fragments in dissociation of energy-selected CH_3F^+ ions at electron binding energies of 16.30, 16.60, 17.00, 17.40 and 18.00 eV have been extracted and displayed in Figure 5(b ~ f). At lower binding energy, in Figure 5(b) and (c), the total KER curves exhibit a peak with large kinetic energy and can be correctly fitted with a Gaussian function. Above the binding energy of 17.00 eV, an additional peak with small kinetic energy can be discerned in the KER curves of Figure 5(d ~ f) that can be modeled with a Boltzmann function.

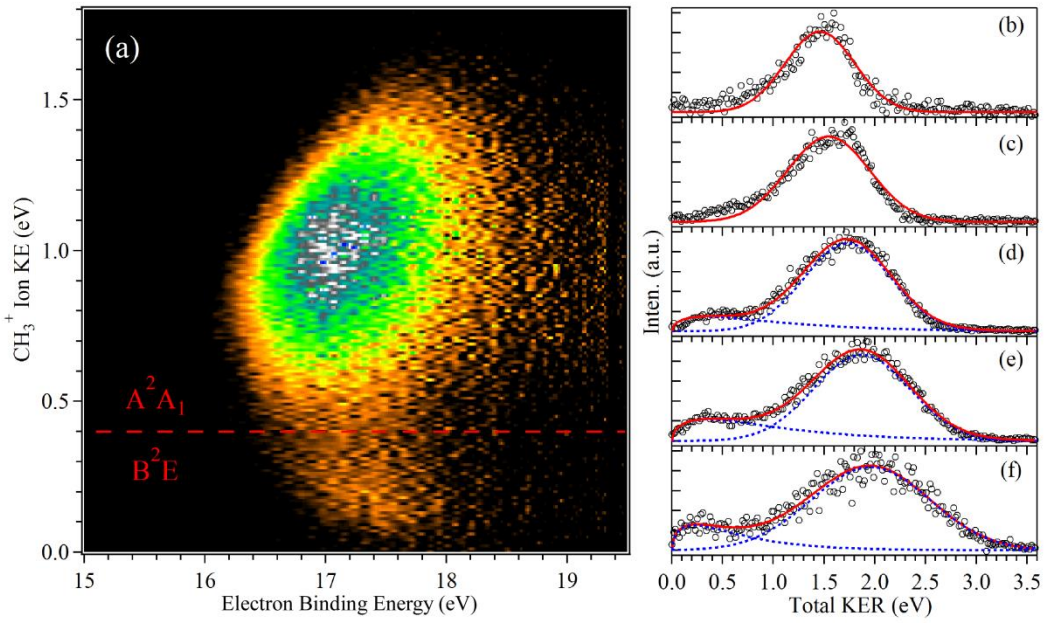

FIG. 5. (a) Electron and ion kinetic energy correlation diagram in dissociation of CH_3F^+ along the CH_3^+ fragmentation channel recorded at hν = 19.50 eV; (b)-(f) Total center of mass KER of the CH_3^+ and F fragments in dissociation of CH_3F^+ at selected electron binding energies of 16.30, 16.60, 17.00, 17.40 and 18.00 eV, the black dots represent the raw data, and the red solid lines correspond to the fitted results with Boltzmann and/or Gaussian functions (blue dotted lines).

The Gaussian function in the total KER curves is attributed to the direct dissociation of the A^2A_1 state and the Boltzmann is correlated to the statistical dissociation from the B^2E state, and are associated with the intense and weak parts of the correlation diagram, respectively.[22] These results show that the totally overlapped A^2A_1 and B^2E states have been disentangled in the correlation diagram and total KER curves. As for CH_3Cl^+, the AIE of the A^2A_1 state of CH_3F^+ has been measured at 16.08 ± 0.03 eV by linear extrapolation of the onset. But for the very weak B^2E state, its AIE can be inferred at 17.00 ± 0.05 eV from the appearance of the Boltzmann component, as seen in Figure 5(a).

4. Conclusion

We have measured the ionization energies of the overlapped A^2A_1 and B^2E electronic states of CH_3Cl^+ and CH_3F^+ ions utilizing the i^{2}PEPICO method[18]. The A^2A_1 and B^2E states overlap in the TPES due to a small energy difference between them and cannot be separated even with a higher energy resolution. However experimental results have shown that the

dissociations of energy-selected CH_3Cl^+ and CH_3F^+ ions in the A^2A_1 and B^2E states are state-specific along the CH_3^+ fragmentation channel. The A^2A_1 state is a repulsive state and a large kinetic energy has been released in dissociation, while the dissociation of the B^2E state is statistical accompanied with a small kinetic energy release. The two A^2A_1 and B^2E states, which overlap if only the excitation energy (hv-eKE) is taken into account, are clearly separated in the electron and ion kinetic energy correlation diagrams based on their different dissociation mechanisms, leading to different KERs, along the CH_3^+ fragmentation channel. This way, the AIEs of the A^2A_1 and B^2E states of CH_3Cl^+ have been measured at 13.67 ± 0.03 and 14.77 ± 0.03 eV, and 16.08 ± 0.03 and 17.00 ± 0.05 eV for CH_3F^+. This method can be generalized to separate ionic states that are otherwise overlapped in normal PES and TPES, especially with the multiplex capabilities of imaging electron/ion coincidence techniques associated with VUV light sources. The latter does not need to be fully continuously tunable, but should allow for the selection of a suitable single energy.

Acknowledgments

We are grateful to J.-F. Gil for his technical support and the SOLEIL staff for smoothly operating the facility and providing beamtime under projects 20130969 and 99140059. X. T. acknowledges support from the National Natural Science Foundation of China (NSFC, 21303177).

References

1 D. W. Turner, C. Baker, A. D. Baker and C. R. Brundle, in *Molecular photoelectron spectroscopy: a handbook of He 584 Å spectra*. Wiley: London, 1970.
2 J. H. D. Eland, in *Photoelectron spectroscopy: an introduction to ultraviolet photoelectron spectroscopy in the gas phase*. Butterworths: London, 1984.
3 I. Powis, T. Baer and C. Y. Ng, in *High Resolution Laser Photoionization and Photoelectron Studies*. Wiley, Chichester, 1995.
4 T. Baer and W. L. Hase, in *Unimolecular Reaction Dynamics: Theory and Experiments*. Oxford University Press, 1996.
5 K. M. Weitzel, G. K. Jarvis, M. Malow, T. Baer, Y. Song and C. Y. Ng, *Phys. Rev. Lett.*, 2001, **86**, 3526-3529.
6 A. F. Lago, J. P. Kercher, A. Bodi, B. Sztaray, B. Miller, D. Wurzelmann and T. Baer, *J. Phys. Chem. A*, 2005, **109**, 1802-1809.

7 G. Meloni, P. Zou, S. J. Klippenstein, M. Ahmed, S. R. Leone, C. A. Taatjes and D. L. Osborn, *J. Am. Chem. Soc.*, 2006, **128**, 13559-13567.
8 Y. Li and F. Qi, *Acc. Chem. Res.*, 2009, **43**, 68.
9 L. F. Luo, X. F. Tang, W. D. Wang, Y. Wang, S. B. Sun, F. Qi and W. X. Huang, *Sci. Rep.*, 2013, **3**, 1.
10 W. Z. Fang, L. Gong, X. B. Shan, F. Y. Liu, Z. Y. Wang and L. S. Sheng, *Anal. Chem.*, 2011, **83**, 9024-9032.
11 J. Kruger, G. A. Garcia, D. Felsmann, K. Moshammer, A. Lackner, A. Brockhinke, L. Nahon and K. Kohse-Hoinghaus, *Phys. Chem. Chem. Phys.*, 2014, **16**, 22791-22804.
12 K. C. Lau and C. Y. Ng, *Acc. Chem. Res.*, 2006, **39**, 823-829.
13 L. A. Curtiss, P. C. Redfern and K. Raghavachari, *J. Chem. Phys.*, 2007, **126**, 084108.
14 C. Y. Ng, *Annu. Rev. Phys. Chem.*, 2002, **53**, 101-140.
15 T. Baer, B. Sztaray, J. P. Kercher, A. F. Lago, A. Bodi, C. Skull and D. Palathinkal, *Phys. Chem. Chem. Phys.*, 2005, **7**, 1507-1513.
16 A. Bodi, P. Hemberger, T. Gerber and B. Sztaray, *Rev. Sci. Instrum.*, 2012, **83**, 083105.
17 G. A. Garcia, H. Soldi-Lose and L. Nahon, *Rev. Sci. Instrum.*, 2009, **80**, 023102.
18 G. A. Garcia, B. K. C. Miranda, M. Tia, S. Daly and L. Nahon, *Rev. Sci. Instrum.*, 2013, **84**, 053112.
19 M. Steinbauer, M. Lang, I. Fischer, B. K. C. de Miranda, C. Romanzin and C. Alcaraz, *Phys. Chem. Chem. Phys.*, 2011, **13**, 17956-17959.
20 X. F. Tang, X. G. Zhou, M. L. Niu, S. L. Liu, J. D. Sun, X. B. Shan, F. Y. Liu and L. S. Sheng, *Rev. Sci. Instrum.*, 2009, **80**, 113101.
21 X. F. Tang, M. L. Niu, X. G. Zhou, S. L. Liu, F. Y. Liu, X. B. Shan and L. S. Sheng, *J. Chem. Phys.*, 2011, **134**, 054312.
22 X. F. Tang, G. A. Garcia and L. Nahon, *J. Phys. Chem. A*, 2015, **doi: 10.1021/jp510319b**.
23 X. F. Tang, X. G. Zhou, M. M. Wu, S. L. Liu, F. Y. Liu, X. B. Shan and L. S. Sheng, *J. Chem. Phys.*, 2012, **136**, 034304.
24 S. M. Gao, Z. Y. Dai, W. Sun, H. Li, J. Wang and Y. X. Mo, *J. Chem. Phys.*, 2013, **139**, 064302.
25 M. Grutter, X. Qian and F. Merkt, *J. Chem. Phys.*, 2012, **137**, 084313.
26 D. M. P. Holland, I. Powis, G. Ohrwall, L. Karlsson and W. von Niessen, *Chem. Phys.*, 2006, **326**, 535-550.
27 H. W. Xi, M. B. Huang, B. Z. Chen and W. Z. Li, *J. Phys. Chem. A*, 2005, **109**, 4381-4387.
28 H. W. Xi, M. B. Huang, B. Z. Chen and W. Z. Li, *J. Phys. Chem. A*, 2005, **109**, 9149-9155.
29 Y. Hikosaka, J. H. D. Eland, T. M. Watson and I. Powis, *J. Chem. Phys.*, 2001, **115**, 4593-4603.
30 R. Locht, B. Leyh, A. Hoxha, D. Dehareng, K. Hottmann, H. W. Jochims and H. Baumgartel, *Chem. Phys.*, 2001, **272**, 293-313.
31 K. M. Weitzel, F. Guthe, J. Mahnert, R. Locht and H. Baumgartel, *Chem. Phys.*, 1995, **201**, 287-298.
32 J. H. D. Eland, R. Frey, A. Kuestler, H. Schulte and B. Brehm, *Int. J. Mass Spectrom. Ion Processes*, 1976, **22**, 155-170.
33 L. Karlsson, R. Jadrny, L. Mattsson, F. T. Chau and K. Siegbahn, *Phys. Scr.*, 1977, **16**, 225-234.
34 I. C. Lane and I. Powis, *J. Phys. Chem.*, 1993, **97**, 5803-5808.
35 A. Lafosse, M. Lebech, J. C. Brenot, P. M. Guyon, O. Jagutzki, L. Spielberger, M. Vervloet, J. C. Houver and D. Dowek, *Phys. Rev. Lett.*, 2000, **84**, 5987-5990.
36 D. Toffoli, R. R. Lucchese, M. Lebech, J. C. Houver and D. Dowek, *J. Chem. Phys.*, 2007, **126**, 054307.

37 L. Nahon, N. Oliveira, G. A. Garcia, J. F. Gil, B. Pilette, O. Marcouille, B. Lagarde and F. Polack, *J. Synchrotron Radiat.*, 2012, **19**, 508-520.
38 A. Eppink and D. H. Parker, *Rev. Sci. Instrum.*, 1997, **68**, 3477.
39 W. C. Wiley and I. H. McLaren, *Rev. Sci. Instrum.*, 1955, **26**, 1150-1157.
40 G. A. Garcia, L. Nahon and I. Powis, *Rev. Sci. Instrum.*, 2004, **75**, 4989-4996.
41 B. Sztaray and T. Baer, *Rev. Sci. Instrum.*, 2003, **74**, 3763-3768.

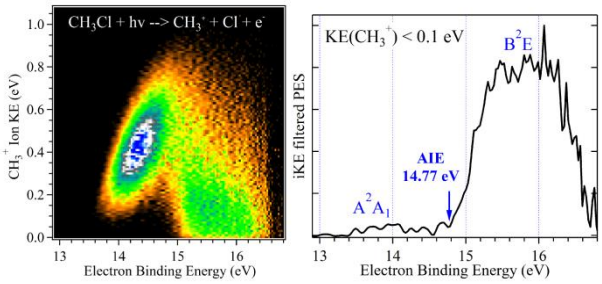

Table of contents. The overlapped A^2A_1 and B^2E electronic states of CH_3Cl^+ have been separated and their adiabatic ionization energies have been measured from electron and ion kinetic energy correlation diagram based on their different dissociation dynamics.